Single nuclei transcriptomics reveal the differentiation trajectories of periosteal skeletal/stem progenitor cells in bone regeneration

Simon Perrin[1], Cécile-Aurore Wotawa[1], Vincent Bretegnier[1], Marine Luka[2,3], Fanny Coulpier[1], Cécile Masson[4,5], Mickael Ménager[2,3], and Céline Colnot[1,*]

[1] Univ Paris Est Creteil, INSERM, IMRB, Creteil, France

[2]Paris Cité University, Imagine Institute, Laboratory of Inflammatory Responses and Transcriptomic Networks in Diseases, Atip-Avenir Team, INSERM UMR 1163, Paris, France.

[3] Labtech Single-Cell@Imagine, Imagine Institute, INSERM UMR 1163, Paris, France.

[4] Bioinformatics Core Facility, Institut Imagine-Structure Fédérative de Recherche Necker, INSERM U1163

[5] INSERM US24/CNRS UAR3633, Paris Cité University, Paris, France

*Corresponding author: celine.colnot@inserm.fr, +33 1 49 81 39 55

Abstract

Bone regeneration is mediated by skeletal stem/progenitor cells (SSPCs) that are mainly recruited from the periosteum after bone injury. The composition of the periosteum and the steps of SSPCs activation and differentiation remain poorly understood. Here, we generated a single-nuclei atlas of the periosteum at steady-state and of the fracture site during early stages of bone repair. We identified periosteal SSPCs expressing stemness markers (Pi16 and Ly6a/Sca1) and responding to fracture by adopting an injury-induced fibrogenic cell (IIFC) fate, prior to undergoing osteogenesis or chondrogenesis. We identified distinct gene cores associated with IIFCs and their engagement into osteogenesis and chondrogenesis involving Notch, Wnt and the circadian clock signaling respectively. Finally, we show that IIFCs are the main source of paracrine signals in the fracture environment, revealing a crucial paracrine role of this transient IIFC population during fracture healing. Overall, our study provides a complete temporal topography of the fracture healing stages and the dynamic response of periosteal SSPCs to injury, redefining our knowledge of bone regeneration.

Graphical Abstract

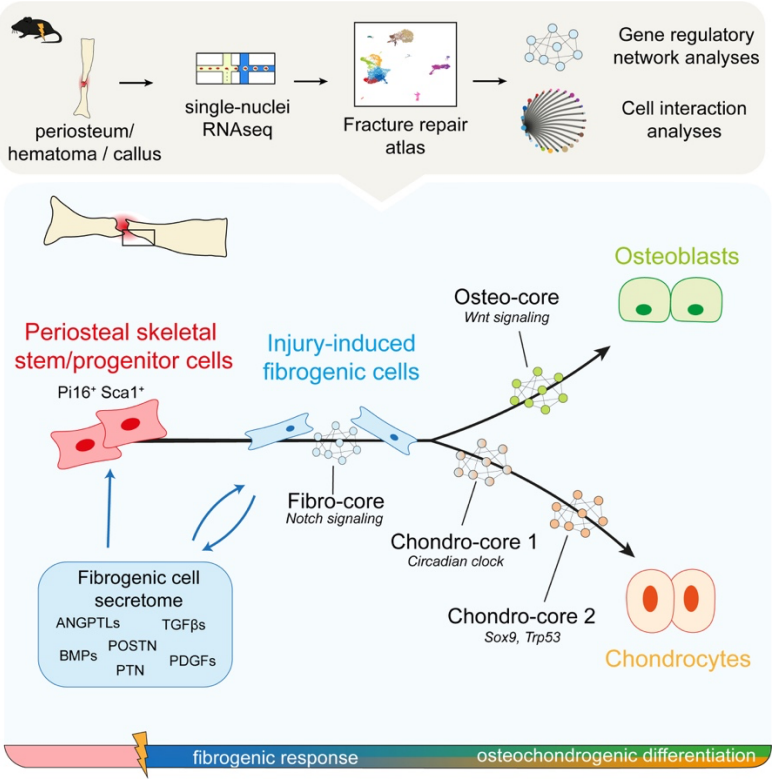

Keywords

periosteum – bone repair – skeletal stem/progenitor cells – single nuclei RNAseq

Introduction

The skeleton provides structural support and protection for internal organs in the vertebrate body. Bones can fracture, but regenerate themselves efficiently without scarring. Bone regeneration is mediated by the action of resident skeletal stem/progenitor cells (SSPCs) from periosteum and bone marrow, and SSPCs from skeletal muscle adjacent to the fracture site[1–4]. SSPCs are activated during the inflammatory phase of healing and differentiate into osteoblasts and/or chondrocytes to repair bone via a combination of intramembranous and endochondral ossification. During intramembranous ossification SSPCs differentiate directly into osteoblasts, while during endochondral ossification SSPCs first differentiate into chondrocytes to form an intermediate cartilage template subsequently replaced by bone.

The periosteum, an heterogenous tissue located on the outer surface of bones, is a crucial source of SSPCs during bone healing[1,2,5–7]. Periosteal SSPCs exhibit a high regenerative potential. They also display a unique osteochondrogenic potential after injury compared to bone marrow SSPCs that are mostly osteogenic and skeletal muscle SSPCs that are mostly chondrogenic[1–4,8]. Periosteal SSPCs (pSSPCs) are still poorly characterized and the origin of their bipotentiality and response to bone injury remain elusive. Recent advances in single cell/nuclei transcriptomic analyses provided new insights in stem cell population heterogeneity and regeneration processes in many organs[9–11]. However, few studies have investigated bone fracture healing at the single cell level and these studies have focused on cultured cells or late stages of bone repair[3,12]. Therefore, a complete dataset of periosteum and bone regeneration is lacking and is essential to decipher the mechanisms of pSSPC activation and regulation. Here, we created a single-nuclei atlas of the uninjured periosteum and its response to bone fracture. We generated single-nuclei RNAseq (snRNAseq) datasets from the uninjured periosteum and from the periosteum and hematoma/callus at days 3, 5 and 7 post-tibial fracture. Our analyses thoroughly describe the heterogeneity of the periosteum at steady state and the steps of pSSPC activation and differentiation after injury. We show that pSSPC represent a single population that can provide osteoblasts and chondrocytes for bone repair

60 by first generating a common injury-induced fibrogenic cell (IIFC) population that can then
61 engage into osteogenesis and chondrogenesis. We identified the gene networks regulating
62 pSSPC fate after injury and IIFCs as the main population producing paracrine factors
63 mediating the initiation of bone healing.

Results

Heterogeneity of the periosteum at steady state

To investigate the heterogeneity of the periosteum at steady-state, we performed snRNAseq of the periosteum of wild-type mice (Fig. 1A-B). After filtering, we obtained 1189 nuclei, corresponding to 8 cell populations: SSPC (expressing *Pi16*), fibroblasts (expressing *Pdgfra*), osteogenic cells (expressing *Runx2*), Schwann cells (expressing *Mpz*), pericytes/SMC (expressing *Tagln*), immune cells (expressing *Ptprc*), adipocytes (expressing *Lpl*), and endothelial cells (ECs, expressing *Pecam1*) (Fig. 1C-D, Fig. S1). We performed in depth analyses of the SSPC, fibroblast and osteogenic cell populations. Subset analyses of clusters 0 to 5 identified 5 distinct SSPC/fibroblast populations expressing *Pdgfra* and *Prrx1*: *Pi16*$^+$, *Csmd1*$^+$*, Hsd11b1*$^+$*, Cldn1*$^+$*,* and *Luzp2*$^+$cells (Fig. 1E-G). *Pi16*$^+$ cells (i.e., cluster 0) were the only cell cluster expressing stemness markers including *Ly6a* (Sca1)*, Dpp4,* and *Cd34* (Fig. 1H). Cytotrace scoring identified *Pi16*$^+$ cells as the population in the most undifferentiated state, suggesting that this population corresponds to periosteal SSPCs (Fig. 1I). We explored the expression of other known markers of periosteal SSPCs, including *Ctsk*, *Acta2* (αSMA), *Gli1*, and *Mx1*, but no marker was fully specific to one cell cluster [1,2,5–7,13–17](Fig. S2).

The fracture repair atlas

To investigate the periosteal response to bone fracture, we collected injured periosteum with hematoma or callus at days 3, 5 and 7 post-fracture, extracted the nuclei and processed them for snRNAseq (Fig. 2A). We combined the datasets with the uninjured periosteum from Figure 1 and obtained a total of 6213 nuclei after filtering. The combined dataset was composed of 25 clusters corresponding to 11 cell populations: SSPCs (expressing *Pi16*), injury-induced fibrogenic cells (IIFC, expressing *Postn*), osteoblasts (expressing *Ibsp*), chondrocytes (expressing *Col2a1*), osteoclasts (expressing *Ctsk*), immune cells (expressing *Ptprc*), Schwann cells (expressing *Mpz*), endothelial cells (expressing *Pecam1*), pericytes (expressing *Rgs5*), SMCs (expressing *Tagln*) and adipocytes (expressing *Lpl*) (Fig. 2B-C, Fig. S3A). Next, we observed the dynamics of the cell populations in response to bone fracture (Fig. 2D, Fig. S3B). After injury, the percentage of SSPCs

93 was strongly decreased and the percentage of IIFCs progressively increased (Fig. 2D-E). The
94 percentage of chondrocytes and osteoblasts increased from day 3 post-fracture. Immune cells
95 were drastically increased at day 3 after injury, before progressively decreasing at days 5 and 7
96 post-fracture (Fig. 2E).
97
98 **Spatial organization of the fracture callus**
99 To evaluate the spatial distribution of the main cell populations identified in the snRNAseq data, we
100 performed in situ immunofluorescence on day 3, 5 and 7 post-fracture hematoma/callus tissues. At
101 day 3 post-fracture, we observed periosteal thickening and the formation of a fibrous hematoma
102 (Fig. 3A). We did not detect SPPCs at both sites, consistent with their absence in day 3 snRNAseq
103 dataset compared to uninjured periosteum. POSTN+ IIFCs and immune cells were the main
104 populations present in hematoma and activated periosteum (Fig. 3B). Few IIFCs in the activated
105 periosteum expressed SOX9 and OSX and only the periosteum was vascularized. At days 5 and
106 7 post-fracture, the callus was formed mainly of fibrotic tissue, bone formed on the periosteal
107 surface at the periphery of the callus and small cartilage islets were detected in the center of the
108 callus near the periosteal surface (Fig. 3C-F). The fibrotic tissue contained mostly IIFCs, as well as
109 immune and endothelial cells. We also observed SOX9+ and OSX+ cells in the fibrotic tissue, while
110 the cartilage was solely composed of SOX9+ chondrocytes. OSX+ osteoblasts were the main cell
111 population detected in the new bone at the periosteal surface. We also observed a progressive
112 reduction of POSTN+ cells and immune cells from day 5 to 7 and increased vascularization in the
113 newly formed bone (Fig. 3C-F).
114
115 **Periosteal SSPCs differentiate via an injury-induced fibrogenic stage.**
116 To understand the differentiation and fate of pSSPCs after fracture, we analyzed the subset of
117 SSPC, IIFC, chondrocyte and osteoblast clusters from the combined fracture dataset (Fig. 4A). We
118 performed pseudotime analyses to determine the differentiation trajectories, defining the starting
119 point in the pSSPC population, where the uninjured and undifferentiated cells cluster. We identified
120 that pSSPC differentiate in 3 stages starting from the pSSPC population (expressing *Ly6a*, *Pi16*
121 and *Cd34*), predominant in uninjured dataset (Fig. 4B-C). Periosteal SSPCs then transition through

122 an injury-induced fibrogenic stage predominant at days 3 and 5 post-injury. In this intermediate
123 fibrogenic stage, pSSPC-derived cells express high levels of extracellular matrix genes, such as
124 *Postn*, *Aspn* and *Tnc*. Later, injury-induced fibrogenic cells (IIFCs) differentiate into chondrocytes
125 (expressing *Acan*, *Col2a1* and *Sox9*) or osteoblasts (expressing *Sp7*, *Alpl* and *Ibsp*), both
126 predominant at days 5 and 7 (Fig. 4B-C, Table S1). These results show that pSSPCs respond to
127 fracture via an injury-induced fibrogenic stage common to chondrogenesis and osteogenesis and
128 independent of their final fate (Fig. 4D). To visualize the transition of IIFCs towards chondrocytes
129 and osteoblasts in the fracture callus, we performed co-immunofluorescence on day 5 post-fracture
130 hematoma/callus. We observed a progressive increase in SOX9 and OSX signals in IIFCs at the
131 fibrosis-to-cartilage and fibrosis-to-bone transition zones respectively (Fig 5A). To functionally
132 validate the steps of pSSPC activation, we isolated SCA1+ GFP+ pSSPCs from *Prx1*^{Cre}*; R26*^{mTmG}
133 mice and grafted them at the fracture site of wild type hosts. We observed that grafted GFP+
134 pSSPCs formed POSTN+ IIFCs at day 5 post-fracture (Fig 5B). Then, we isolated GFP+ IIFCs from
135 the fracture callus of *Prx1*^{Cre}*; R26*^{mTmG} mice at day 3 post fracture and grafted the GFP+ IIFCs at
136 the fracture site of wild type hosts. We showed that grafted cells formed bone and cartilage at day
137 14 post-fracture. These results confirmed that pSSPCs first become IIFCs that differentiate into
138 osteoblasts and chondrocytes.
139
140 **Characterization of injury-activated fibrogenic cells**
141 We performed in depth analyses of the newly identified IIFC population. Gene ontology (GO)
142 analyses of upregulated genes in IIFCs (clusters 2 to 6) showed enrichment in GOs related to
143 tissue development, extracellular matrix (ECM), and ossification (Fig. 6A). We identified several
144 ECM-related genes specifically upregulated in IIFCs, including collagens (*Col3a1, Col5a1, Col8a1,*
145 *Col12a1*), *Postn*, and *Aspn* (Fig. 6B-C). We also identified GO terms related to cell signaling,
146 migration, differentiation, and proliferation, indicating that this step corresponds to an injury-induced
147 activation. To further understand the mechanisms regulating SSPC activation and fate after injury,
148 we performed gene regulatory network (GRN) analyses on the subset of SSPCs, IIFCs, osteoblasts
149 and chondrocytes using SCENIC package (Single Cell rEgulatory Network Inference and
150 Clustering)[18]. We identified 280 activated regulons (transcription factor/TF and their target genes)

151 in the subset dataset. We performed GRN-based tSNE clustering and identified SSPC, IIFC,
152 chondrocyte and osteoblast populations (Fig. 6D-E, Fig. S4A). Fibroblasts from uninjured
153 periosteum (*Hsd11b1*$^{+}$*, Cldn1*$^{+}$ and *Luzp2*$^{+}$ cells) clustered separately from the other population,
154 indicating the absence of their contribution to bone healing. Analysis of the number of activated
155 regulons per cell indicated that SSPCs are the most stable cell population (higher number of
156 activated regulons), while IIFCs are the less stable population, confirming their transient state (Fig.
157 6F). We then investigated cell population specific regulons. SSPCs showed activated regulons
158 linked to stemness, including Hoxa10 (16g), Klf4 (346g), Pitx1 (10g), and Mta3 (228g) [19–21], and
159 immune response, including Stat6 (30g), Fiz1 (72g) and Stat5b (18g)[22–24] (Fig. 6G). Osteoblasts
160 and chondrocytes display cell specific activated regulons including Sp7 (18g) and Sox9 (77g)
161 respectively. We identified 21 regulons that we named fibro-core and that were upregulated
162 specifically in the IIFC population (Fig. 6F-I, Table S2). Several fibro-core regulons, such as Meis1
163 (1556g), Pbx1 (11g), Six1 (20g), and Pbx3 (188g) are known to be involved in cell differentiation
164 during tissue development and repair[25–28]. Reactome pathway analysis showed that the most
165 significant terms linked to IIFC-specific TFs are related to Notch signaling (Fig. 6J, Table S3). We
166 confirmed that Notch signaling is specifically increased in the IIFC stage (Fig. 6K), suggesting its
167 involvement in the fibrogenic phase of bone repair.
168
169 **Distinct gene cores regulate the engagement of IIFCs into chondrogenesis and osteogenesis**
170 We sought to identify the drivers of the transition of IIFCs to chondrocytes or osteoblasts. We
171 identified 2 cores of regulons involved in chondrogenic differentiation. Chondro-core 1 is composed
172 of 9 regulons specific to the transition of IIFC to chondrocytes, including Maf (17g), Arntl (1198g),
173 and Nfatc2 (37g) and chondro-core 2, composed of 14 regulons specific to differentiated
174 chondrocytes (Fig. 7A, Fig. S4B). Chondro-core 1 regulons are known to be regulators of the
175 circadian clock (Npas2, Arntl) or of the T/B-cell receptor cellular response (Bach2, Nfact2, Nfkb1).
176 STRING network analysis showed that TFs from the chondro-core 1 are interacting between each
177 other and are at the center of the interactions between the chondro-core 2 TFs, including Sox9,
178 Trp53 and Mef2c (Fig. 7B, Fig S4C). We observed that chondro-core 1 is only transiently activated
179 when IIFCs are engaging into chondrogenesis and precedes the activation of chondro-core 2 (Fig.

180 7C-D). Chondro-core 1 activity was high in early differentiated chondrocytes (low *Acan* expression)
181 and progressively reduced as chondrocytes undergo differentiation, while chondro-core 2 activity
182 was gradually increased as chondrocytes differentiate (Fig. 7D). This suggests that transient
183 activation of the chondro-core 1 allows the transition of IIFCs into chondrocytes. Then, we
184 investigated the osteogenic commitment of IIFCs. We identified 8 regulons forming the osteo-core
185 and activated in IIFCs transitioning to osteoblasts, such as Tcf7 (23g), Bcl11b (14g), and Tbx2
186 (36g) (Fig. 7E, Fig. S4D). STRING network analysis showed that the genes with the strongest
187 interaction with the osteo-core TFs are mostly related to Wnt signaling (Fig. 7F). This reveals the
188 role of Wnt signaling in this transition from early fibrogenic activation of pSSPCs to osteogenic
189 differentiation during bone repair. We calculated the osteo-core activity, and observed that it is
190 gradually increased and maintained in osteogenic cells, showing that the osteo-core is required for
191 the transition and maturation of IIFC into osteoblasts (Fig 7G-H). Overall, we identified distinct
192 cores of regulons with distinct dynamics driving the transition of IIFCs into chondrocytes and
193 osteoblasts.
194
195 **IIFCs mediate paracrine interactions during bone repair**
196 Paracrine cell interactions are crucial drivers of tissue regeneration and stem cell activation. To
197 identify key cell interactions during bone repair, we performed cell interaction analyses using
198 CellChat package[29]. We observed that IIFCs are the predominant source of outgoing signals during
199 bone repair, and are also important receivers of signals, highlighting their central role in mediating
200 cell interactions after fracture (Fig. 8A-B). Endothelial cells were mostly receiving signaling, while
201 chondrocytes, osteoblasts and most immune cells exhibited reduced interactions with the other cell
202 types in the fracture environment. IIFCs interact with all cell populations in the fracture environment,
203 but the strongest interactions were with SSPCs and IIFCs (Fig. S5A). CellChat analyses of the
204 subset of SSPCs, IIFCs, osteoblasts and chondrocytes confirmed that IIFCs are the major source
205 and receiver population of paracrine signalings after fracture (Fig. S5B). We then analyzed the
206 main secreted factors from IIFCs. IIFCs secreted periostin (*Postn*), BMPs (*Bmp5*), pleiotropin/PTN
207 (*Ptn*), TGFβs (*Tgfb2*, *Tgfb3*), PDGFs (*Pdgfc*, *Pdgfd*) and angiopoietin-likes/ANGPTLs (*Angplt2,*
208 *Angplt4*) (Fig. 8C-D, Fig. S5C). We observed differences in the dynamics of these factors, as some

209 of them peak at day 3 post-fracture such as TGFβ, while others peak at day 5 such as BMP,
210 POSTN, PTN and ANGPLT (Fig. 8E). We assessed the dynamics of ligand and receptor expression
211 and observed that ligand expression was specific of the IIFC phase and of the fracture response
212 (Fig. 8F). Receptor expression was high in both SSPCs and IIFCs, and receptors were expressed
213 from steady state, suggesting that SSPCs can receive signals from IIFCs. Analysis of SSPC
214 incoming signals confirmed that IIFCs are the major source of paracrine factors for SSPCs (Fig.
215 8G), indicating that they contribute to SSPC recruitment after fracture.

Discussion

The periosteum is the main driver of bone regeneration. Yet the periosteum composition and its response to bone fracture are poorly described. Here, we used single-nuclei transcriptomics to understand the heterogeneity of the periosteum at steady state and the changes occurring within periosteum after bone fracture. We developed a protocol to extract nuclei from freshly dissected periosteum, allowing to capture their intact transcriptomic profile without enzymatic digestion-induced stress[30–32]. In addition, we performed snRNAseq without sorting specific populations, allowing the identification of all cell types located in the periosteum and the fracture environment from the early stages of repair. Our study provides the first complete fracture repair atlas, a key tool to understand bone regeneration.

First, we described the heterogeneity of the periosteum at steady state. While previous studies performed scRNAseq on sorted periosteal cell populations, our dataset uncovers the diversity of cell populations within the periosteum. We describe fibroblast populations, as well as tissue resident immune cells, adipocytes, and blood vessel/nerve-related cells. We identified one SSPC population of undifferentiated cells expressing markers such as Sca1, *Dpp4* and *Pi16,* known to mark fibroblasts with stemness potential[33]. No markers previously described such as *Ctsk*, or *Gli1* were fully specific of one cell cluster and of the undifferentiated SSPC population, suggesting that these markers may label heterogenous cell populations[2,5,6,15].

After fracture, the composition of the periosteum changes drastically, with the appearance of IIFC and immune cells from day 3 post-fracture, and of chondrocytes and osteoblasts from day 5 post-fracture. Previous studies based on in vitro analyses and in vivo lineage tracing demonstrated that the periosteum displays the unique potential to form both bone and cartilage after fracture[1,3,5]. Yet, it was still unknown if the periosteum contains a bipotent SSPC population or several SSPC populations with distinct potentials after injury. Here, we show that pSSPCs activate and form bone and cartilage via a single trajectory emerging from Sca1+ SSPCs. Periosteal Sca1+ SSPCs become IIFCs, a state marked by a decreased expression of stemness markers and a strong expression of extracellular matrix genes, such as *Postn* and *Aspn* and activation of Notch-related

246 TFs. Thus, bone injury does not induce an expansion of Sca1+ SSPCs, rather a transition toward
247 IIFCs that progressively expand and represent the main cell population within the fracture callus
248 until day 7 post-fracture. Following this unique fibrogenic step, IIFCs undergo either osteogenesis
249 or chondrogenesis. This newly identified transient IIFC state represents the crossroad of bone
250 regeneration and SSPC differentiation.
251
252 GRN analyses identified TFs regulating SSPC response to fracture. We found that Notch signaling
253 was specific to the injury-induced fibrogenic phase. Previous studies reported the role of Notch and
254 Wnt in osteogenesis, and their temporal separation during intramembranous ossification [8,34,35]. Our
255 results show that Notch/Wnt activation after fracture correlates with the successive stages of
256 pSSPC fibrogenic and osteogenic differentiation. However, we discover that Wnt is only
257 upregulated in IIFCs engaging into osteogenesis, while Notch is activated early in IIFCs prior to
258 their commitment to osteogenesis or chondrogenesis. In addition, we identified a chondro-core of
259 9 regulons transiently activated when IIFCs engage into chondrogenesis. Among these regulons,
260 several are involved in the autonomous circadian clock, including *Npas2* and *Arntl* (Bmal1). Bmal1
261 was previously shown to be a regulator of cartilage differentiation in bone development and
262 homeostasis[36]. Bmal1 inactivation leads to chondrocyte apoptosis and disruption of signaling
263 involved in cartilage formation, including TGFβ, Ihh, HIF1α and NFAT[37–40]. This suggests a role of
264 the circadian clock genes as key regulators of chondrogenesis during bone repair. IIFCs are also
265 crucial regulators of the fracture paracrine environment. IIFCs secrete factors including BMPs,
266 PDGFs, TGFβs, and POSTN, known to be required for successful bone healing[1,3,14,41]. These
267 signals allow IIFCs to interact with all cell types in the fracture environment, but primarily with
268 SSPCs and others IIFCs. Thus, IIFCs are contributing to the recruitment of SSPCs and promoting
269 their own maturation and differentiation.
270
271 Overall, our study provides a complete dataset of the early steps of bone regeneration. The newly
272 identified SSPC activation pattern shows the importance of the temporal dynamic of cell
273 phenotypes and signaling pathways after injury. IIFCs appear as a transient cell population that
274 plays essential roles in the initial steps of bone repair. Deeper understanding of IIFC regulation will

275 be crucial as they represent the ideal target to enhance bone healing and potentially treat bone
276 repair defects.
277

Materials and Methods

Mice

C57BL/6ScNj were obtained from Janvier Labs (France). *Prx1*^{Cre} [42] and *Rosa26-mtdTomato-mEGFP* (*R26*^{mTmG})[43] were obtained from Jackson Laboratory (Bar Harbor, ME).). All SSPCs, including pSSPCs, are marked by GFP in *Prx1*$^{Cre;}$ R26^{mTmG} mice. Mice were bred in animal facilities at IMRB, Creteil and kept in separated ventilated cages, in pathogen-controlled environment and ad libitum access to water and food. All procedures performed were approved by Paris Est Creteil University Ethical Committee. Twelve-week-old males and females were mixed in experimental groups.

Tibial fracture

Open non-stabilized tibial fractures were induced as previously described [44]. Mice were anesthetized with an intraperitoneal injection of Ketamine (50 mg/mL) and Medetomidine (1 mg/kg) and received a subcutaneous injection of Buprenorphine (0.1 mg/kg) for analgesia. Mice were kept on a 37°C heating pad during anesthesia. The right hindlimb was shaved and sanitized. The skin was incised to expose the tibia and osteotomy was performed in the mid-diaphysis by cutting the bone. The wound was sutured, the mice were revived with an intraperitoneal injection of atipamezole (1 mg/kg) and received two additional analgesic injections in the 24 hours following surgery. Mice were sacrificed 3, 5, 7 or 14 days post-fracture.

Nuclei extraction

Nuclei extraction protocol was adapted from [45,46]. We generated 4 datasets for this study: uninjured periosteum, periosteum and hematoma at days 3, 5 and 7 post-tibial fracture. The uninjured and day 3 post-fracture datasets were generated in duplicates. For uninjured periosteum, tibias from 4 mice were dissected free of muscle and surrounding tissues. The epiphyses were cut and the bone marrow flushed. The periosteum was scraped from the cortex using dissecting Chisel (10095-12, Fine Science Tools). For days 3, 5 and 7 post fracture, injured tibias from 4 to 9 mice were collected and the surrounded tissues were removed. The activated periosteum was scraped and collected with the hematoma. Collected tissues were minced and placed 5 min in ice-cold Nuclei Buffer

307 (NUC101, Merck) before mechanical nuclei extraction using a glass douncer. Extraction was
308 performed by 20 strokes of pestle A followed by 5-10 of pestle B. Nuclei suspension was filtered,
309 centrifuged and resuspended in RNAse-free PBS (AM9624, ThermoFischer Scientific) with 2%
310 Bovine Serum Albumin (A2153, Merck) and 0.2 U/µL RNAse inhibitor (3335399001, Roche). A
311 second step of centrifugation was performed to reduce contamination by cytoplasmic RNA. Sytox™
312 AADvanced™ (S10349, ThermoFischer Scientific) was added (1/200) to label nuclei and Sytox-
313 AAD+ nuclei were sorted using Sony SH800.
314

315 **Single nuclei RNA sequencing**

316 The snRNA-seq libraries were generated using Chromium Single Cell Next GEM 3′ Library & Gel
317 Bead Kit v.3.1 (10x Genomics) according to the manufacturer's protocol. Briefly, 10 000 to 20 000
318 nuclei were loaded in the 10x Chromium Controller to generate single-nuclei gel-beads in emulsion.
319 After reverse transcription, gel-beads in emulsion were disrupted. Barcoded complementary DNA
320 was isolated and amplified by PCR. Following fragmentation, end repair and A-tailing, sample
321 indexes were added during index PCR. The purified libraries were sequenced on a Novaseq
322 (Illumina) with 28 cycles of read 1, 8 cycles of i7 index and 91 cycles of read 2. Sequencing data
323 were processed using the Cell Ranger Count pipeline and reads were mapped on the mm10
324 reference mouse genome with intronic and exonic sequences.
325

326 **Filtering and clustering using Seurat**

327 Single-nuclei RNAseq analyses were performed using Seurat v4.1.0 [47,48] and Rstudio v1.4.1717.
328 Aligned snRNAseq datasets were filtered to retain only nuclei expressing between 200 et 5000
329 genes and expressing less than 2% of mitochondrial genes and 1.5% of ribosomal genes.
330 Contamination from myogenic cells were removed from the analyses. After filtering, we obtained
331 1378 nuclei from uninjured periosteum, 1634 from day 3 post-fracture, 2089 from d5 post-fracture
332 and 1112 from day 7 post-fracture. The replicates of the uninjured dataset were integrated using
333 Seurat. The integrated dataset was regressed on cell cycle, mitochondrial and ribosomal content
334 and clustering was performed using the first 15 principal components and a resolution of 0.5.
335 SSPC/fibroblast and osteogenic cells were isolated and reclustered using the first 10 principal

336 components and a resolution of 0.2. Uninjured, d3, d5 and d7 datasets were integrated using
337 Seurat. The integrated dataset was regressed on cell cycle, mitochondrial and ribosomal content.
338 Clustering was performed using the first 20 principal components and a resolution of 1.3. SSPC,
339 IIFC, chondrogenic and osteogenic clusters from the integration were isolated to perform subset
340 analysis. The subset was reclustered using the first 15 principal components and a resolution of
341 0.6.
342
343 **Pseudotime analysis using monocle3**
344 Monocle3 v1.0.0 was used for pseudotime analysis [49]. Single-cell trajectories were determined
345 using monocle3 default parameters. The starting point of the pseudotime trajectory was determined
346 as the cells from the uninjured dataset with the highest expression of stem/progenitor marker genes
347 *(Ly6a, Cd34, Dpp4, Pi16)*. Pseudotime value were added in Seurat object as metadata and used
348 with Seurat package.
349
350 **Differentiation state analysis using Cytrotrace**
351 To assess the level of differentiation of the cell clusters, we performed analyses using CytoTrace
352 with the default parameters. Cytotrace scoring was plotted in violon plot and on the Seurat UMAP
353 clustering.
354
355 **Gene Ontology and Reactome and analyses**
356 Reactome and GO analyses were performed using EnrichR [50]. All significant GO terms from
357 upregulated genes in clusters 2 to 6 of the subset of SSPCs, IIFCs, osteoblasts and chondrocytes
358 were manually categorized. The 5 more significant terms of the Reactome analysis from the
359 fibrogenic TFs of Fig. 6 are presented in Table S3.
360
361 **Single cell regulatory network inference using SCENIC**
362 Single cell regulatory network inference and clustering (SCENIC) [18] was used to infer transcription
363 factor (TF) networks active in SSPCs, IIFCs, osteoblasts and chondrocytes. Analysis was
364 performed using recommended parameters using the packages SCENIC v1.3.1, AUCell v1.16.0,

365 and RcisTarget v1.14 and the motif databases RcisTarget and GRNboost. SCENIC package was
366 used to perform regulon based tSNE clustering and identified population specific regulons.
367
368 **Cell-cell interaction using CellChat**
369 Cell communication analysis was performed using the R package CellChat[29] with default
370 parameters on the complete fracture combined dataset and on the subset of SSPCs, IIFCs,
371 osteoblasts and chondrocytes.
372
373 **STRING network analyses**
374 To assess protein-protein interaction network, we used the STRING v11.5 database[51]. To assess
375 interaction in the chondro-core, we performed the analysis on the chondro-core and chondro-
376 specific TFs identified in our analysis. For osteo-core analyses, we performed the analysis with
377 osteo-core genes and the most significant interactions.
378
379 **Histology and immunofluorescence**
380 Mouse samples were processed as previously described[44]. Tibias were collected and fixed in 4% PFA
381 (sc-281692, CliniSciences) for 4 hours at 4°C. Then, samples were decalcified in 19% EDTA for 10
382 days (EU00084, Euromedex), cryoprotected in 30% sucrose (200-301-B, Euromedex) for 24h and
383 embedded in OCT. Samples were sectioned in 10µm thick sections. Cryosections were defrosted
384 and rehydrated in PBS. For Safranin-O staining, sections were stained with Weigert's solution for
385 5 min, rinsed in running tap water for 3 min and stained with 0.02% Fast Green for 30 seconds
386 (F7252, Merck), followed by 1% acetic acid for 30 seconds and Safranin'O solution for 45 min
387 (S2255, Merck). For immunofluorescence, sections were incubated 1 hour at room temperature in
388 5% serum, 0.25% Triton PBS before incubation overnight at 4°C with the following antibodies: Rat
389 monoclonal to mouse Sca1 (740450, BD Biosciences), Rabbit monoclonal to mouse SOX9
390 (ab185230, Abcam), Rabbit polyclonal to mouse Osterix/Sp7 (ab22552, Abcam), Goat polyclonal
391 to mouse Periostin (AF2955, R&D Systems), Goat polyclonal to mouse PECAM1 (AF3628,
392 Biotechne), Rat monoclonal to mouse CD45 (552848, BD Bioscience). Secondary antibody

393 incubation was performed at room temperature for 1 hour. Slides were mounted with Fluoromount-
394 G mounting medium with DAPI (00-4959-52, Life Technologies).
395
396 **Tissue dissociation and cell sorting**
397 *Periosteal SSPC isolation*
398 To isolate periosteal cells, uninjured tibias from *Prx1^{Cre}; R26^{mTmG}* mice were collected and all
399 surrounding soft tissues were carefully removed. Epiphyses were embedded in low melting agarose and
400 tibias were placed for 30 min at 37°C in digestion medium composed of PBS with 3mg/ml of Collagenase
401 B (C6885, Merck), 4mg/ml of Dispase (D4693, Merck) and 100U/mL of DNAse I (WOLS02007, Serlabo,
402 France). After digestion, tibias were removed and the suspension was filtered, centrifuged and
403 resuspend.
404
405 *Injury-induced fibrogenic cell isolation*
406 The fracture hematoma and the activated periosteum were collected from *Prx1^{Cre}; R26^{mTmG}* mice 3 days
407 post-fracture. Tissues were minced and digested at 37°C for 2 hours in DMEM (21063029, Life
408 Technologies) with 1% Trypsin (15090046, Life Technologies) and 1% collagenase D (11088866001,
409 Roche). Cells in suspension were removed every 20 min and digestion medium was replaced. After 2
410 hours, the cell suspension was filtered, centrifuged and resuspended.
411
412 *Cell sorting and transplantation*
413 Digested cells were incubated 30 minutes with anti-Sca1-BV650 (BD Biosciences, 740450) or anti-
414 CD146-BV605 (BD Biosciences, 740636). Cells were sorted using Influx Cell Sorter. Prior sorting, Sytox
415 Blue (S34857, Thermo Fisher Scientific) was added to stain dead cells. For pSSPCs, living single GFP+
416 Sca1+ cells were sorted. For IIFCs, living single GFP+ CD146- cells were sorted. Cell transplantation
417 was performed as described in[44]. 30000 to 45000 sorted GFP+ cells were embedded in Tisseel Prima
418 fibrin gel, composed of fibrinogen and thrombin (3400894252443, Baxter S.A.S, USA), according to
419 manufacturer's instructions. Briefly, the cells were resuspended in 15 µL of fibrin (diluted at 1/4), before
420 adding 15 µL of thrombin (diluted at 1/4) and mixing. The pellet was then placed on ice at least 15 min
421 for polymerization. The cell pellet was transplanted at the fracture site of wild type mice at the time of
422 fracture.

423

424 **Statistical analyses**

425 Statistical difference between the number of activated regulons per cell was determined using one

426 way-ANOVA followed by post-hoc test. A p-value < 0.001 is reported as ***.

427

Resource availability

Single nuclei RNAseq datasets are deposited in the Gene Expression Omnibus (GSE234451). This paper does not report original code. Further information and request for resources and reagents should be directed to and will be fulfilled by the lead contact, Céline Colnot (celine.colnot@inserm.fr).

Acknowledgements

This work was supported by ANR-18-CE14-0033, ANR-21-CE18-007-01 to C.C., NIAMS R01 AR072707 to C. C. and Ted Miclau, R01 AR081671 to C.C. and Ralph Marcucio. S. Perrin was supported by a PhD fellowship from Paris Cité University. We thank O. Pellé from the Flow Cytometry platform at Imagine Institute and all the staff from the Imagine genomic core facility at Imagine Institute. We thank A. Julien, S. Protic, M. Ethel, C. Goachet and Y. Hachemi for technical assistance or advice.

Conflict of interests

Authors declare no competing interests.

Author contributions

Conceptualization: S.P. and C.C. Methodology: S.P. and C.C. Formal analysis: S.P. and C-A.W. Investigation: S.P., M.L., F.C. and C.M. Resources: F.C. and M.M. Writing – Original Draft: S.P. and C.C. Visualization: S.P. Supervision: C.C. Project administration: C.C. Funding Acquisition: C.C

445 **References**

446 1. Duchamp de Lageneste, O. *et al.* Periosteum contains skeletal stem cells with high bone
447 regenerative potential controlled by Periostin. *Nat Commun* **9**, 773 (2018).
448 2. Jeffery, E. C., Mann, T. L. A., Pool, J. A., Zhao, Z. & Morrison, S. J. Bone marrow and periosteal
449 skeletal stem/progenitor cells make distinct contributions to bone maintenance and repair. *Cell Stem*
450 *Cell* **29**, 1547-1561.e6 (2022).
451 3. Julien, A. *et al.* Skeletal stem/progenitor cells in periosteum and skeletal muscle share a
452 common molecular response to bone injury. *J of Bone & Mineral Res* jbmr.4616 (2022)
453 doi:10.1002/jbmr.4616.
454 4. Julien, A. *et al.* Direct contribution of skeletal muscle mesenchymal progenitors to bone repair.
455 *Nature Communications* **12**, 2860 (2021).
456 5. Debnath, S. *et al.* Discovery of a periosteal stem cell mediating intramembranous bone
457 formation. *Nature* **562**, 133–139 (2018).
458 6. Matthews, B. G. *et al.* Heterogeneity of murine periosteum progenitors involved in fracture
459 healing. *eLife* **10**, e58534 (2021).
460 7. Ortinau, L. C. *et al.* Identification of Functionally Distinct Mx1+αSMA+ Periosteal Skeletal Stem
461 Cells. *Cell Stem Cell* **25**, 784-796.e5 (2019).
462 8. Matsushita, Y. *et al.* A Wnt-mediated transformation of the bone marrow stromal cell identity
463 orchestrates skeletal regeneration. *Nat Commun* **11**, 332 (2020).
464 9. De Micheli, A. J. *et al.* Single-Cell Analysis of the Muscle Stem Cell Hierarchy Identifies
465 Heterotypic Communication Signals Involved in Skeletal Muscle Regeneration. *Cell Rep* **30**, 3583-
466 3595.e5 (2020).
467 10. Guerrero-Juarez, C. F. *et al.* Single-cell analysis reveals fibroblast heterogeneity and myeloid-
468 derived adipocyte progenitors in murine skin wounds. *Nat Commun* **10**, 650 (2019).
469 11. Storer, M. A. *et al.* Acquisition of a Unique Mesenchymal Precursor-like Blastema State
470 Underlies Successful Adult Mammalian Digit Tip Regeneration. *Developmental Cell* **52**, 509-524.e9
471 (2020).
472 12. Sivaraj, K. K. *et al.* Mesenchymal stromal cell-derived septoclasts resorb cartilage during
473 developmental ossification and fracture healing. *Nat Commun* **13**, 571 (2022).
474 13. Tournaire, G. *et al.* Nestin-GFP transgene labels skeletal progenitors in the periosteum. *Bone*
475 **133**, 115259 (2020).

476 14. Gao, B. *et al.* Macrophage-lineage TRAP+ cells recruit periosteum-derived cells for periosteal
477 osteogenesis and regeneration. *Journal of Clinical Investigation* **129**, 2578–2594 (2019).
478 15. Chan, C. K. F. *et al.* Identification and Specification of the Mouse Skeletal Stem Cell. *Cell* **160**,
479 285–298 (2015).
480 16. He, X. *et al.* Sox9 positive periosteal cells in fracture repair of the adult mammalian long bone.
481 *Bone* **103**, 12–19 (2017).
482 17. Böhm, A.-M. *et al.* Activation of Skeletal Stem and Progenitor Cells for Bone Regeneration Is
483 Driven by PDGFRβ Signaling. *Developmental Cell* **51**, 236-254.e12 (2019).
484 18. Aibar, S. *et al.* SCENIC: single-cell regulatory network inference and clustering. *Nat Methods*
485 **14**, 1083–1086 (2017).
486 19. Leclerc, K. *et al.* Hox genes are crucial regulators of periosteal stem cell identity. *Development*
487 **150**, dev201391 (2023).
488 20. Nemec, S. *et al.* Pitx1 directly modulates the core limb development program to implement
489 hindlimb identity. *Development* **144**, 3325–3335 (2017).
490 21. Takahashi, K. & Yamanaka, S. Induction of pluripotent stem cells from mouse embryonic and
491 adult fibroblast cultures by defined factors. *Cell* **126**, 663–676 (2006).
492 22. Chen, H. *et al.* Activation of STAT6 by STING is critical for antiviral innate immunity. *Cell* **147**,
493 436–446 (2011).
494 23. Kollmann, S. *et al.* A STAT5B-CD9 axis determines self-renewal in hematopoietic and leukemic
495 stem cells. *Blood* **138**, 2347–2359 (2021).
496 24. Tsuruyama, T. *et al.* Dual retrovirus integration tagging: identification of new signaling molecules
497 Fiz1 and Hipk2 that are involved in the IL-7 signaling pathway in B lymphoblastic lymphomas. *J Leukoc*
498 *Biol* **88**, 107–116 (2010).
499 25. Le Grand, F. *et al.* Six1 regulates stem cell repair potential and self-renewal during skeletal
500 muscle regeneration. *J Cell Biol* **198**, 815–832 (2012).
501 26. Linares, A. J. *et al.* The splicing regulator PTBP1 controls the activity of the transcription factor
502 Pbx1 during neuronal differentiation. *eLife* **4**, e09268 (2015).
503 27. Rottkamp, C. A., Lobur, K. J., Wladyka, C. L., Lucky, A. K. & O'Gorman, S. Pbx3 is required for
504 normal locomotion and dorsal horn development. *Dev Biol* **314**, 23–39 (2008).
505 28. Wang, S. *et al.* Meis1 Controls the Differentiation of Eye Progenitor Cells and the Formation of

506 Posterior Poles during Planarian Regeneration. *Int J Mol Sci* **24**, 3505 (2023).
507 29. Jin, S. *et al.* Inference and analysis of cell-cell communication using CellChat. *Nat Commun* **12**,
508 1088 (2021).
509 30. Ding, J. *et al.* Systematic comparison of single-cell and single-nucleus RNA-sequencing
510 methods. *Nat Biotechnol* **38**, 737–746 (2020).
511 31. Machado, L. *et al.* Tissue damage induces a conserved stress response that initiates quiescent
512 muscle stem cell activation. *Cell Stem Cell* **28**, 1125-1135.e7 (2021).
513 32. van den Brink, S. C. *et al.* Single-cell sequencing reveals dissociation-induced gene expression
514 in tissue subpopulations. *Nat Methods* **14**, 935–936 (2017).
515 33. Buechler, M. B. *et al.* Cross-tissue organization of the fibroblast lineage. *Nature* **593**, 575–579
516 (2021).
517 34. Lee, S. *et al.* Notch-Wnt signal crosstalk regulates proliferation and differentiation of
518 osteoprogenitor cells during intramembranous bone healing. *npj Regen Med* **6**, 29 (2021).
519 35. Wang, C. *et al.* NOTCH signaling in skeletal progenitors is critical for fracture repair. *Journal of*
520 *Clinical Investigation* **126**, 1471–1481 (2016).
521 36. Chen, G. *et al.* The biological function of BMAL1 in skeleton development and disorders. *Life*
522 *Sciences* **253**, 117636 (2020).
523 37. Dudek, M. *et al. The clock transcription factor BMAL1 is a key regulator of extracellular matrix*
524 *homeostasis and cell fate in the intervertebral disc*.
525 http://biorxiv.org/lookup/doi/10.1101/2023.02.12.528214 (2023) doi:10.1101/2023.02.12.528214.
526 38. Dudek, M. *et al.* The chondrocyte clock gene Bmal1 controls cartilage homeostasis and integrity.
527 *Journal of Clinical Investigation* **126**, 365–376 (2015).
528 39. Ma, Z. *et al.* Deletion of clock gene Bmal1 impaired the chondrocyte function due to disruption
529 of the HIF1α-VEGF signaling pathway. *Cell Cycle* **18**, 1473–1489 (2019).
530 40. Takarada, T. *et al.* Clock Genes Influence Gene Expression in Growth Plate and Endochondral
531 Ossification in Mice. *Journal of Biological Chemistry* **287**, 36081–36095 (2012).
532 41. Xia, C. *et al.* TGF-β/Smad2 signalling regulates enchondral bone formation of Gli1 $^{+}$ periosteal
533 cells during fracture healing. *Cell Prolif* **53**, (2020).
534 42. Logan, M. *et al.* Expression of Cre recombinase in the developing mouse limb bud driven by
535 aPrxl enhancer. *genesis* **33**, 77–80 (2002).

536 43. Muzumdar, M. D., Tasic, B., Miyamichi, K., Li, L. & Luo, L. A global double-fluorescent Cre
537 reporter mouse. *Genesis* **45**, 593–605 (2007).
538 44. Perrin, S., Julien, A., Duchamp de Lageneste, O., Abou-Khalil, R. & Colnot, C. Mouse Periosteal
539 Cell Culture, in vitro Differentiation, and in vivo Transplantation in Tibial Fractures. *BIO-PROTOCOL* **11**,
540 (2021).
541 45. Santos, M. D. *et al.* Extraction and sequencing of single nuclei from murine skeletal muscles.
542 *STAR Protocols* **2**, 100694 (2021).
543 46. G Martelotto, L. *'Frankenstein' protocol for nuclei isolation from fresh and frozen tissue for*
544 *snRNAseq v2*. https://www.protocols.io/view/frankenstein-protocol-for-nuclei-isolation-from-f-3fkgjkw
545 (2019) doi:10.17504/protocols.io.3fkgjkw.
546 47. Stuart, T. *et al.* Comprehensive Integration of Single-Cell Data. *Cell* **177**, 1888-1902.e21 (2019).
547 48. Butler, A., Hoffman, P., Smibert, P., Papalexi, E. & Satija, R. Integrating single-cell
548 transcriptomic data across different conditions, technologies, and species. *Nat Biotechnol* **36**, 411–420
549 (2018).
550 49. Cao, J. *et al.* The single-cell transcriptional landscape of mammalian organogenesis. *Nature*
551 **566**, 496–502 (2019).
552 50. Kuleshov, M. V. *et al.* Enrichr: a comprehensive gene set enrichment analysis web server 2016
553 update. *Nucleic Acids Res* **44**, W90-97 (2016).
554 51. Szklarczyk, D. *et al.* The STRING database in 2021: customizable protein-protein networks, and
555 functional characterization of user-uploaded gene/measurement sets. *Nucleic Acids Res* **49**, D605–
556 D612 (2021).
557
558

Figures

Figure 1

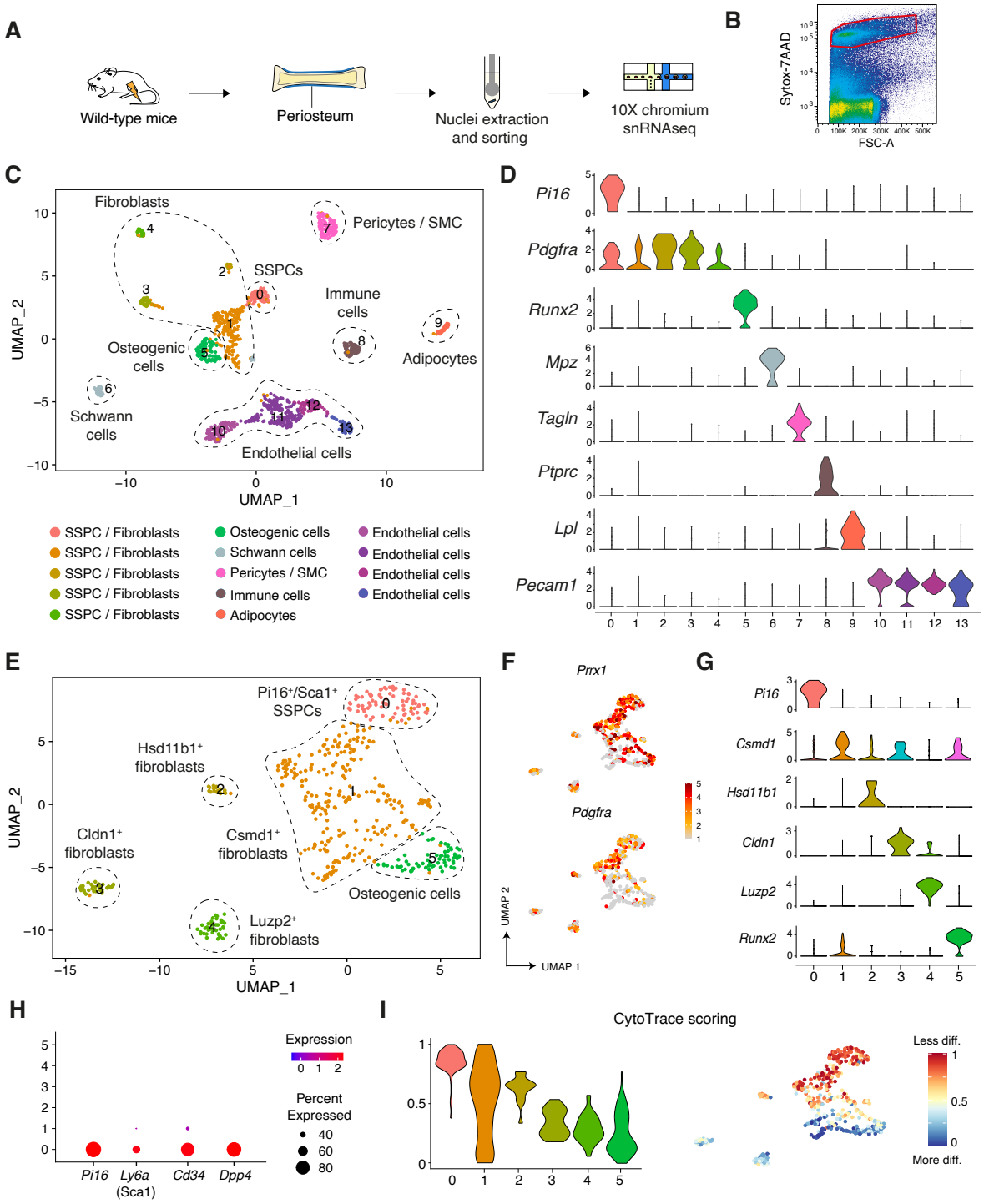

562 **Figure 1: Heterogeneity of the periosteum at steady state**

563 **A.** Experimental design. Nuclei were extracted from the periosteum of uninjured tibia and processed for
564 single-nuclei RNAseq. **B.** Sorting strategy of nuclei stained with Sytox-7AAD for snRNAseq. Sorted
565 nuclei are delimited by a red box. **C.** UMAP projection of color-coded clustering of the uninjured
566 periosteum dataset. Six populations are identified and delimited by black dashed lines. **D.** Violin plots of
567 key marker genes of the different cell populations. **E.** UMAP projection of color-coded clustering of the
568 subset of SSPC/fibroblasts. **F.** Feature plots of *Prrx1* and *Pdgfra* in the subset of SSPC/fibroblasts. **G.**
569 Feature plots of key marker genes of the different cell populations. **H.** Dot plot of the stemness markers
570 *Pi16, Ly6a* (Sca1*), Cd34,* and *Dpp4*. **I.** Violin and feature plots of Cytotrace scoring in the subset of
571 SSPC/fibroblasts, showing that Sca1+ SSPCs (cluster 0) are the less differentiated cells in the dataset.
572

Figure 2

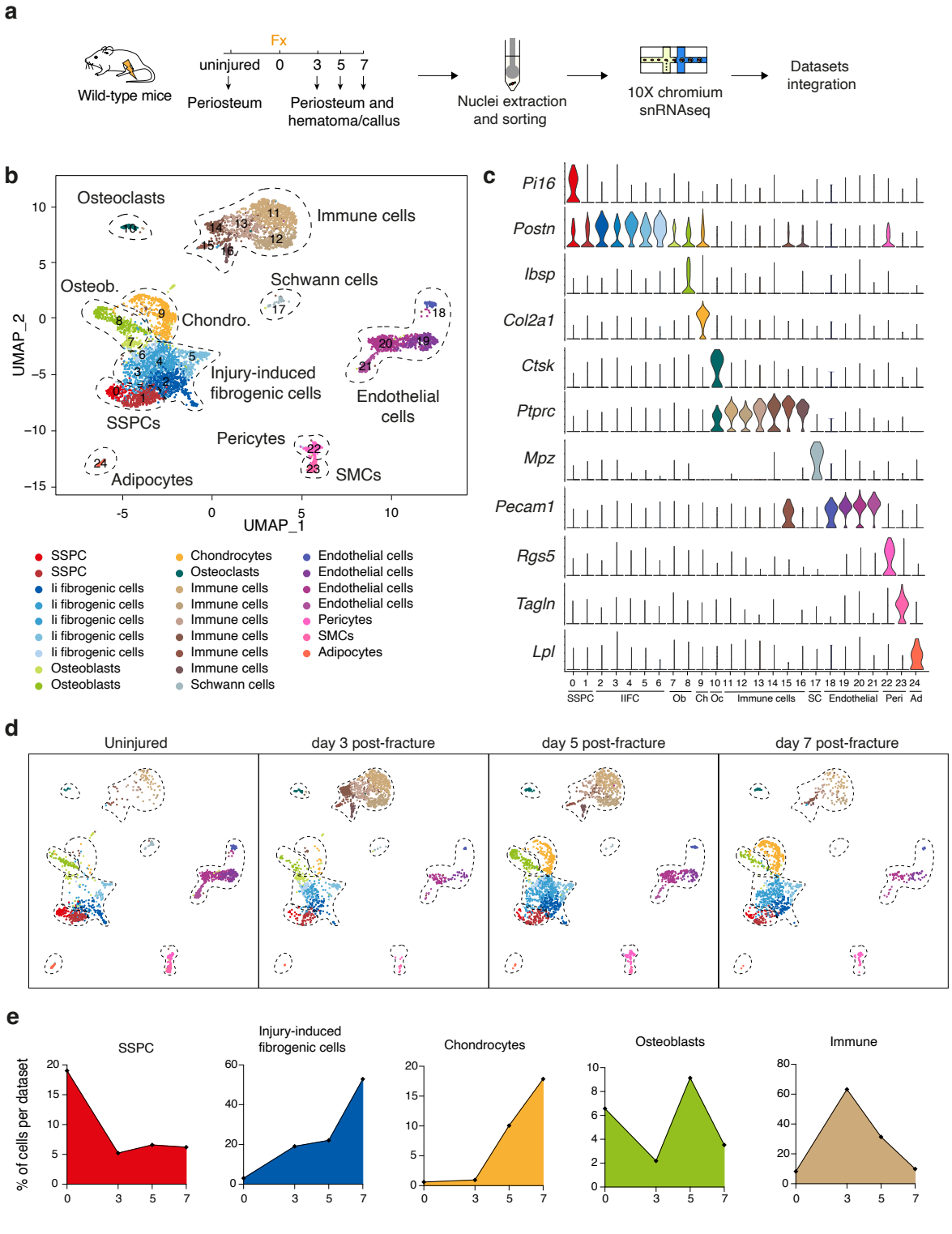
a
Wild-type mice
Fx
uninjured 0 3 5 7
Periosteum
Periosteum and hematoma/callus
Nuclei extraction and sorting
10X chromium snRNAseq
Datasets integration
b
Osteoclasts
Immune cells
Schwann cells
Osteob.
Chondro.
Injury-induced fibrogenic cells
Endothelial cells
SSPCs
Pericytes
SMCs
Adipocytes
UMAP_2
UMAP_1
SSPC
SSPC
Ii fibrogenic cells
Ii fibrogenic cells
Ii fibrogenic cells
Ii fibrogenic cells
Ii fibrogenic cells
Osteoblasts
Osteoblasts
Chondrocytes
Osteoclasts
Immune cells
Immune cells
Immune cells
Immune cells
Immune cells
Immune cells
Schwann cells
Endothelial cells
Endothelial cells
Endothelial cells
Endothelial cells
Pericytes
SMCs
Adipocytes
c
Pi16
Postn
Ibsp
Col2a1
Ctsk
Ptprc
Mpz
Pecam1
Rgs5
Tagln
Lpl
SSPC
IIFC
Ob
Ch Oc
Immune cells
SC
Endothelial
Peri
Ad
d
Uninjured
day 3 post-fracture
day 5 post-fracture
day 7 post-fracture
e
% of cells per dataset
SSPC
Injury-induced fibrogenic cells
Chondrocytes
Osteoblasts
Immune

575 **Figure 2: Periosteal response to fracture at single-nuclei resolution**

576 **A.** Experimental design. Nuclei were extracted from the periosteum of uninjured tibia of wild-type mice
577 and from the periosteum and hematoma at days 3, 5 and 7 post-tibial fracture and processed for single-
578 nuclei RNAseq. **B.** UMAP projection of color-coded clustering of the integration of uninjured, day 3, day
579 5 and day 7 datasets. Eleven populations are identified and delimited by black dashed lines. **C.** Violin
580 plots of key marker genes of the different cell populations. **D.** UMAP projection of the combined dataset
581 separated by time-point. **E.** Percentage of cells in SSPC, injury-induced fibrogenic cell, osteoblast,
582 chondrocyte, and immune cell clusters in uninjured, day 3, day 5 and day 7 datasets.
583

Figure 3

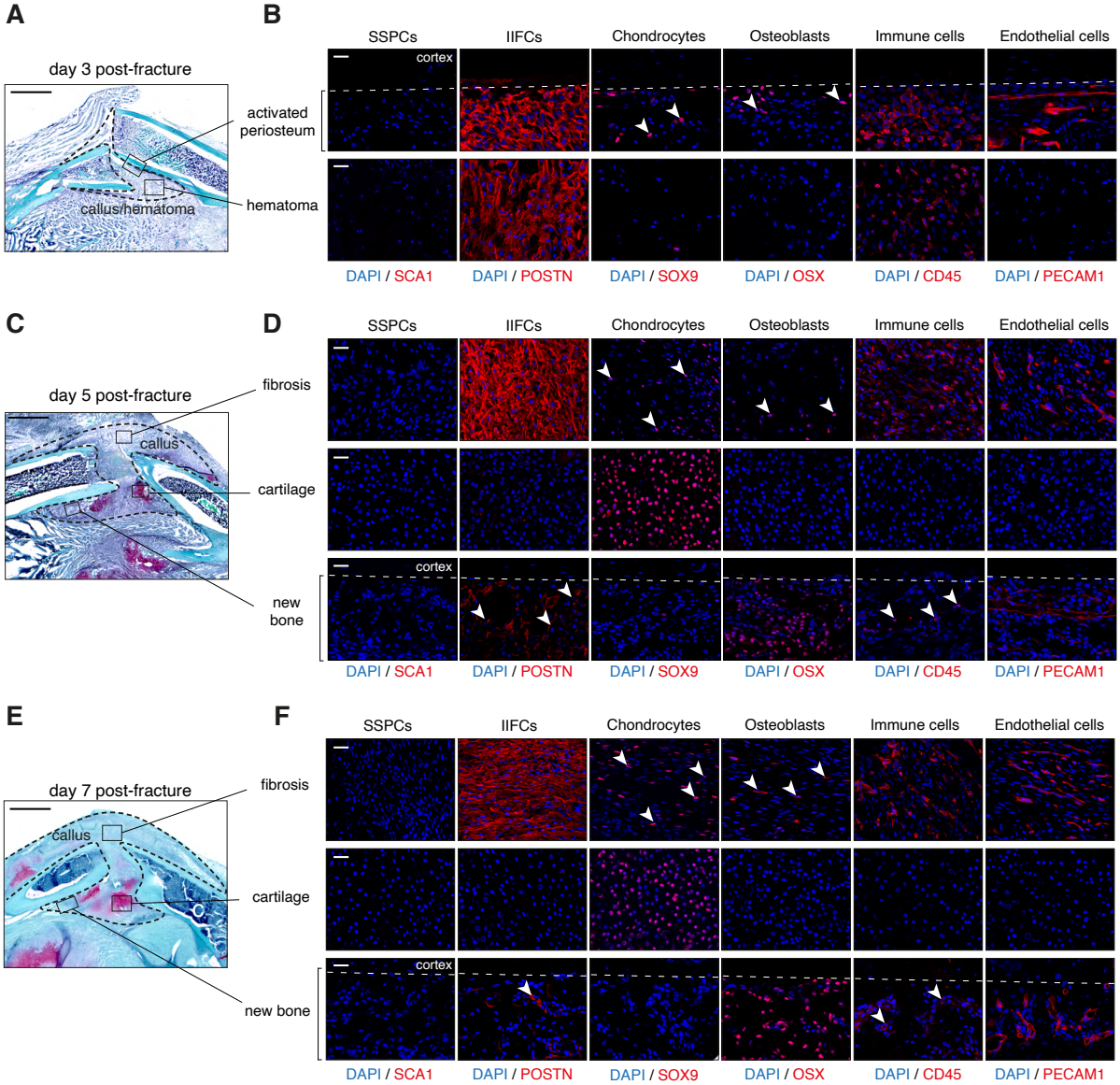
A
B
day 3 post-fracture
activated periosteum
hematoma
callus/hematoma
SSPCs
IIFCs
Chondrocytes
Osteoblasts
Immune cells
Endothelial cells
cortex
DAPI / SCA1
DAPI / POSTN
DAPI / SOX9
DAPI / OSX
DAPI / CD45
DAPI / PECAM1
C
D
day 5 post-fracture
fibrosis
callus
cartilage
new bone
E
F
day 7 post-fracture

584

585

586 **Figure 3: Cellular organization of the fracture callus**

587 **A.** Safranin'O staining of longitudinal callus sections at day 3-post tibial fracture. **B**. Immunofluorescence
588 on adjacent sections show absence of SSPCs (SCA1$^+$), and presence of IIFCs (POSTN$^+$) and immune
589 cells (CD45$^+$) in the activated periosteum and hematoma at day 3-post fracture. Chondrocytes (SOX9$^+$,
590 arrowhead), osteoblasts (OSX$^+$, arrowhead) and endothelial cells (PECAM1$^+$) are detected in activation
591 periosteum (n=3 per group). **C.** Safranin'O staining of longitudinal callus sections at day 5-post tibial
592 fracture. **D**. Immunofluorescence on adjacent sections show IIFCs (POSTN$^+$), chondrocytes (SOX9$^+$,
593 arrowhead), osteoblasts (OSX$^+$, arrowhead), immune cells (CD45$^+$) and endothelial cells (PECAM1$^+$) in
594 the fibrosis, chondrocytes (SOX9$^+$) in cartilage and osteoblasts (OSX$^+$), immune cells (CD45$^+$,
595 arrowhead) and endothelial cells (PECAM1$^+$) in new bone. (n=3 per group). **E.** Safranin'O staining of
596 longitudinal callus sections at day 7-post tibial fracture. **F**. Immunofluorescence on adjacent sections
597 show IIFCs (POSTN$^+$), chondrocytes (SOX9$^+$, arrowhead), osteoblasts (OSX$^+$, arrowhead), immune
598 cells (CD45$^+$) and endothelial cells (PECAM1$^+$) in the fibrosis, chondrocytes (SOX9$^+$) in cartilage and
599 osteoblasts (OSX$^+$), immune cells (CD45$^+$, arrowhead) and endothelial cells (PECAM1$^+$) in new bone
600 (n=3 per group). Scale bars: A-B-E: 1mm, B-D-F: 100μm.
601

Figure 4

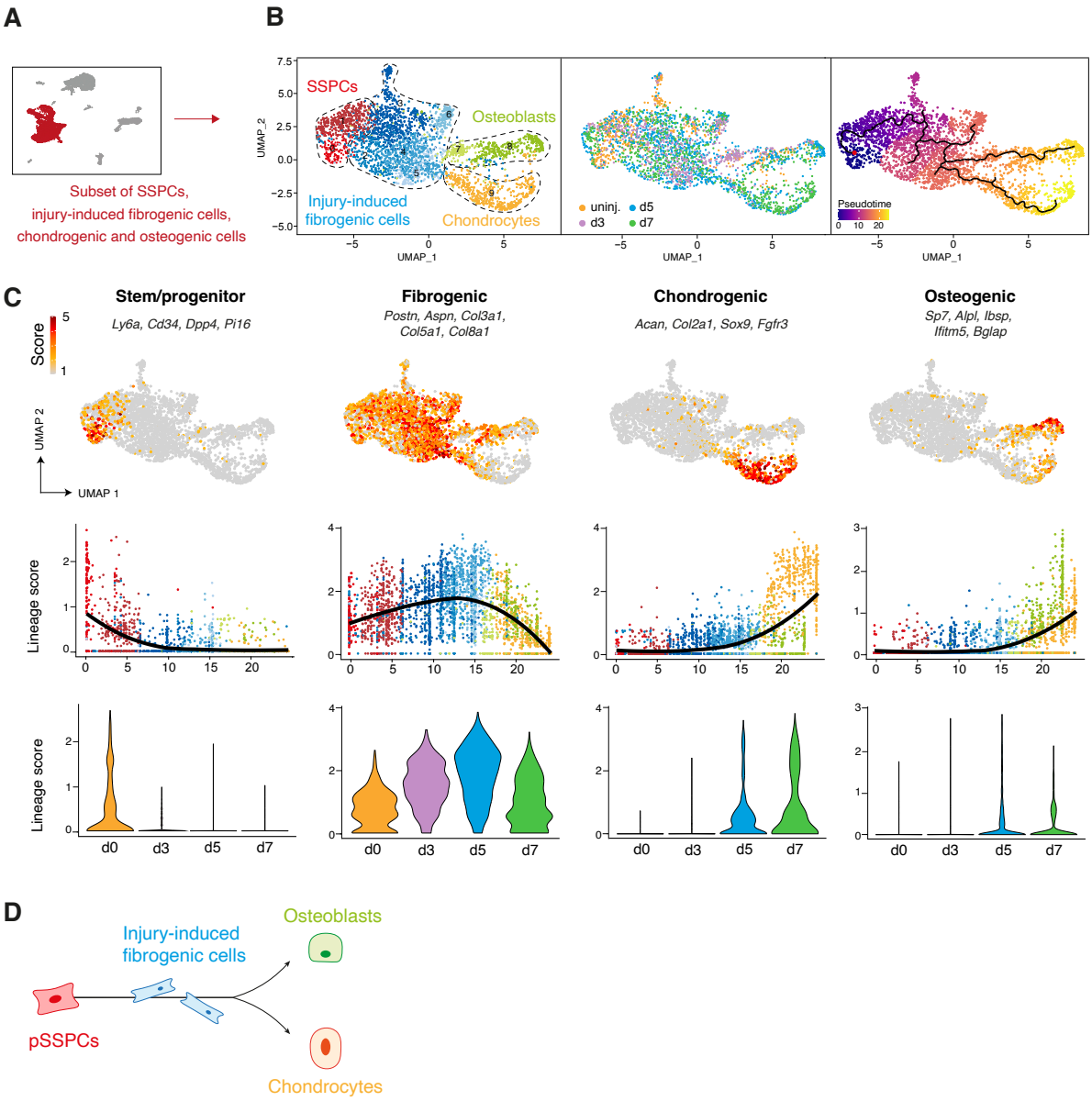
A
Subset of SSPCs,
injury-induced fibrogenic cells,
chondrogenic and osteogenic cells
B
SSPCs
Osteoblasts
Injury-induced
fibrogenic cells
Chondrocytes
UMAP_2
UMAP_1
uninj.
d3
d5
d7
Pseudotime
C
Stem/progenitor
Ly6a, Cd34, Dpp4, Pi16
Fibrogenic
Postn, Aspn, Col3a1,
Col5a1, Col8a1
Chondrogenic
Acan, Col2a1, Sox9, Fgfr3
Osteogenic
Sp7, Alpl, Ibsp,
Ifitm5, Bglap
Score
UMAP 2
UMAP 1
Lineage score
d0
d3
d5
d7
D
Injury-induced
fibrogenic cells
Osteoblasts
pSSPCs
Chondrocytes

604 **Figure 4: Periosteal SSPCs activate through a common fibrogenic state prior to undergoing**
605 **osteogenesis or chondrogenesis**

606 **A.** SSPCs, injury-induced fibrogenic cells (IIFCs), chondrocytes and osteoblasts from integrated
607 uninjured, day 3, day 5 and day 7 post-fracture samples were extracted for a subset analysis. **B.** UMAP
608 projection of color-coded clustering (left), color-coded sampling (middle) and monocle pseudotime
609 trajectory (right) of the subset dataset. The four populations are delimited by black dashed lines. **C.** (top)
610 Feature plots of the stem/progenitor, fibrogenic chondrogenic and osteogenic lineage scores (middle)
611 Scatter plot of the lineage scores along pseudotime. (bottom) Violon plot of the lineage score per time
612 point. **D.** Schematic representation of the activation trajectory of pSSPCs after fracture.
613

Figure 5

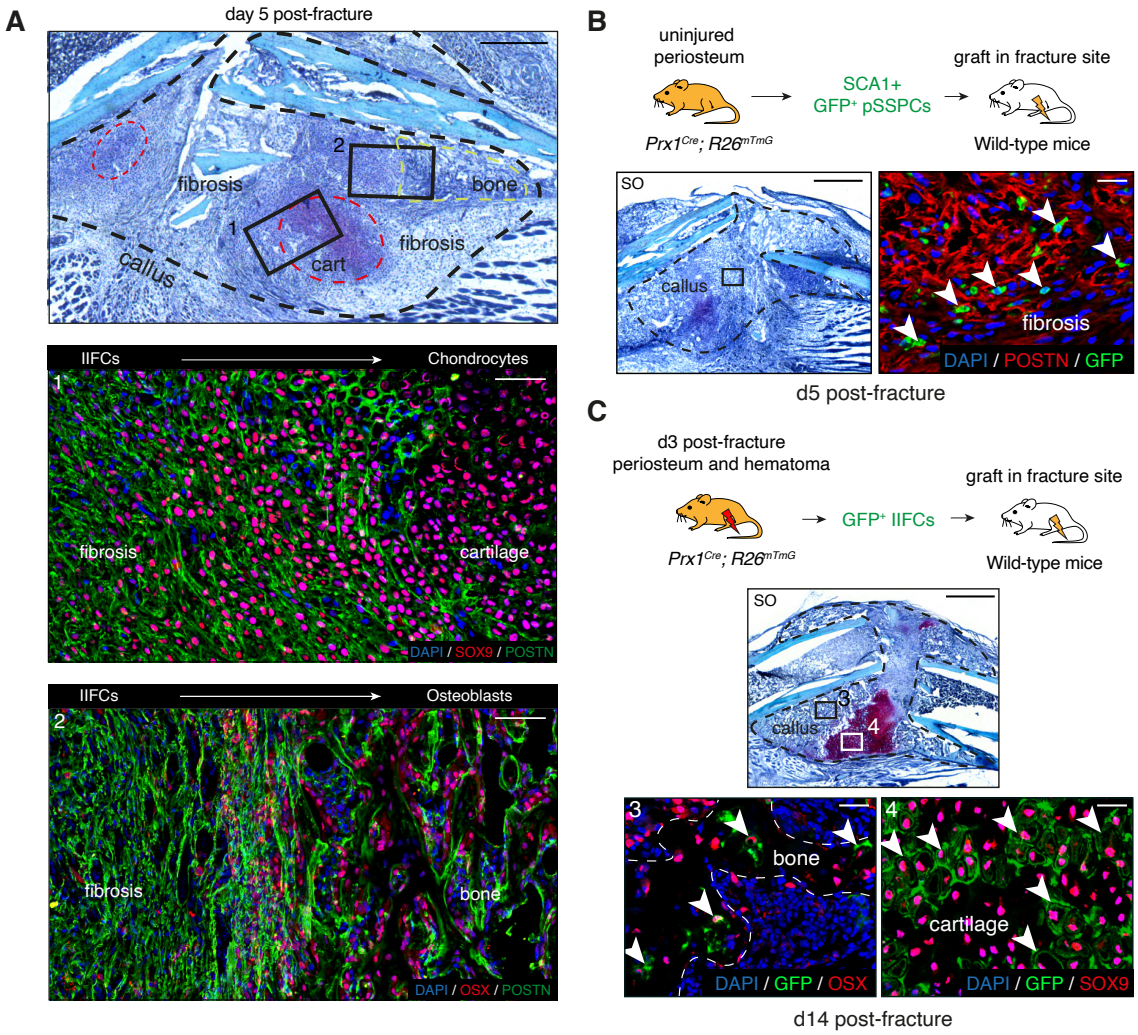
A
day 5 post-fracture
fibrosis
bone
callus
cart
fibrosis
IIFCs
Chondrocytes
fibrosis
cartilage
DAPI / SOX9 / POSTN
IIFCs
Osteoblasts
fibrosis
bone
DAPI / OSX / POSTN
B
uninjured periosteum
SCA1+ GFP+ pSSPCs
graft in fracture site
Prx1Cre; R26mTmG
Wild-type mice
SO
callus
fibrosis
DAPI / POSTN / GFP
d5 post-fracture
C
d3 post-fracture periosteum and hematoma
GFP+ IIFCs
graft in fracture site
Prx1Cre; R26mTmG
Wild-type mice
SO
callus
bone
cartilage
DAPI / GFP / OSX
DAPI / GFP / SOX9
d14 post-fracture

614

615 **Figure 5: In vivo validation of pSSPC activation trajectory**

616 **A**. (Top) Representative Safranin'O staining on longitudinal sections of the hematoma/callus at day 5
617 post-fracture. The callus is composed of fibrosis, cartilage (red dashed line) and bone (green dashed
618 line). (Middle, box 1) Immunofluorescence on adjacent section shows decreased expression of POSTN
619 (green) and increased expression of SOX9 (red) in the fibrosis-to-cartilage transition zone. (Bottom, box
620 2) Immunofluorescence on adjacent section shows decreased expression of POSTN (green) and
621 increased expression of OSX (red) in the fibrosis-to-bone transition zone (n=3 per group). **B.**
622 Experimental design: GFP+ Sca1+ SSPCs were isolated from uninjured tibia of *Prx1*^{Cre}*; R26*^{mTmG} mice
623 and grafted at the fracture site of wild type mice. Safranin'O staining of callus sections at day 5 post-
624 fracture and high magnification of POSTN immunofluorescence of adjacent section showing that GFP+
625 cells contribute to the callus and that grafted SSPCs differentiate into POSTN+ IIFCS (white
626 arrowheads) (n=4 per group). **C.** Experimental design: GFP+ IIFCs from day 3 post-fracture tibia were
627 isolated from *Prx1*^{Cre}*; R26*^{mTmG} mice and grafted at the fracture site of wild type mice. Safranin'O of
628 callus sections at day 14 post-fracture and high magnification of OSX and SOX9 immunofluorescence
629 of adjacent sections showing that GFP+ cells contribute to the callus and that grafted IIFCs differentiate
630 into OSX+ osteoblasts (box 3, white arrowheads) and SOX9+ chondrocytes (box 4, white arrowheads)
631 (n=4 per group). Scale bars: Low magnification: A: 500μm, B-C: 1mm. High magnification: 100μm.
632

Figure 6

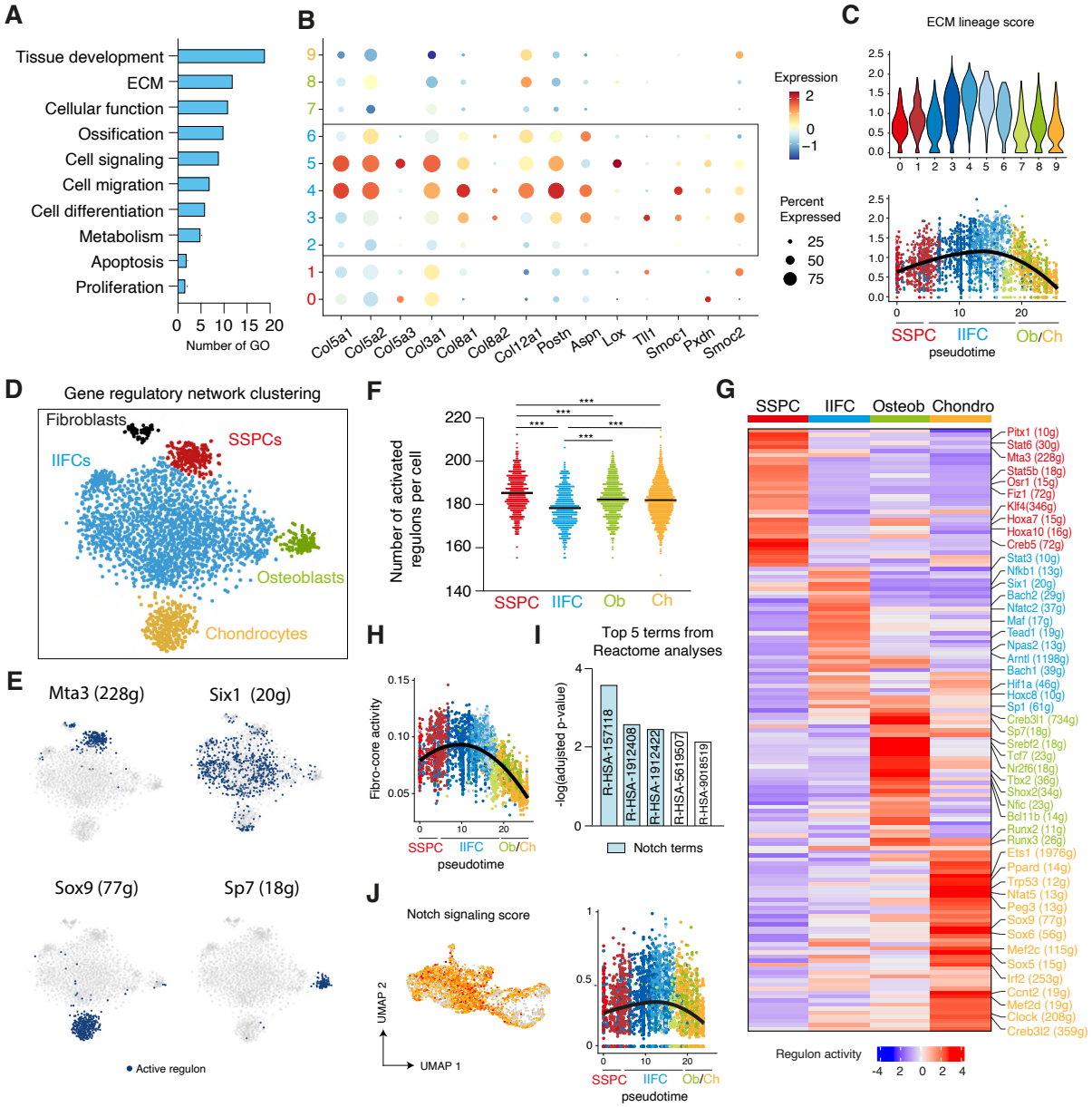

633
634

635 **Figure 6: Characterization of injury-activated fibrogenic cells**

636 **A.** Gene ontology analyses of upregulated genes in IIFCs (clusters 2 to 6 of UMAP clustering from Fig.
637 4). **B.** Dot plot of ECM genes in UMAP clustering from Fig. 4. **C.** Feature plot per cluster and scatter
638 plot along pseudotime of the mean expression of ECM genes. **D.** Gene regulatory network (GRN)-based
639 tSNE clustering of the subset of SSPCs, IIFCs, chondrocytes and osteoblasts. **E.** Activation of Mta3,
640 Six1, Sox9 and Sp7 regulons in SSPCs, IIFCs, chondrocytes and osteoblasts. Blue dots mark cells with
641 active regulon. **F.** Number of regulons activated per cell in the SSPC, IIFC, osteoblast (Ob) and
642 chondrocyte (Ch) populations. Statistical differences were calculated using one-way ANOVA. ***: p-
643 value < 0.001. **G.** Heatmap of activated regulons in SSPC, IIFC, osteoblast and chondrocyte
644 populations. **H.** Scatter plot of the activity of the combined fibrogenic regulons along monocle
645 pseudotime from Fig. 4. **I.** Reactome pathway analyses of the fibrogenic regulons shows that the 3 most
646 significant terms are related to Notch signaling (blue). **J.** Feature plot in Seurat clustering and scatter
647 plot along monocle pseudotime of the Notch signaling score.
648

Figure 7

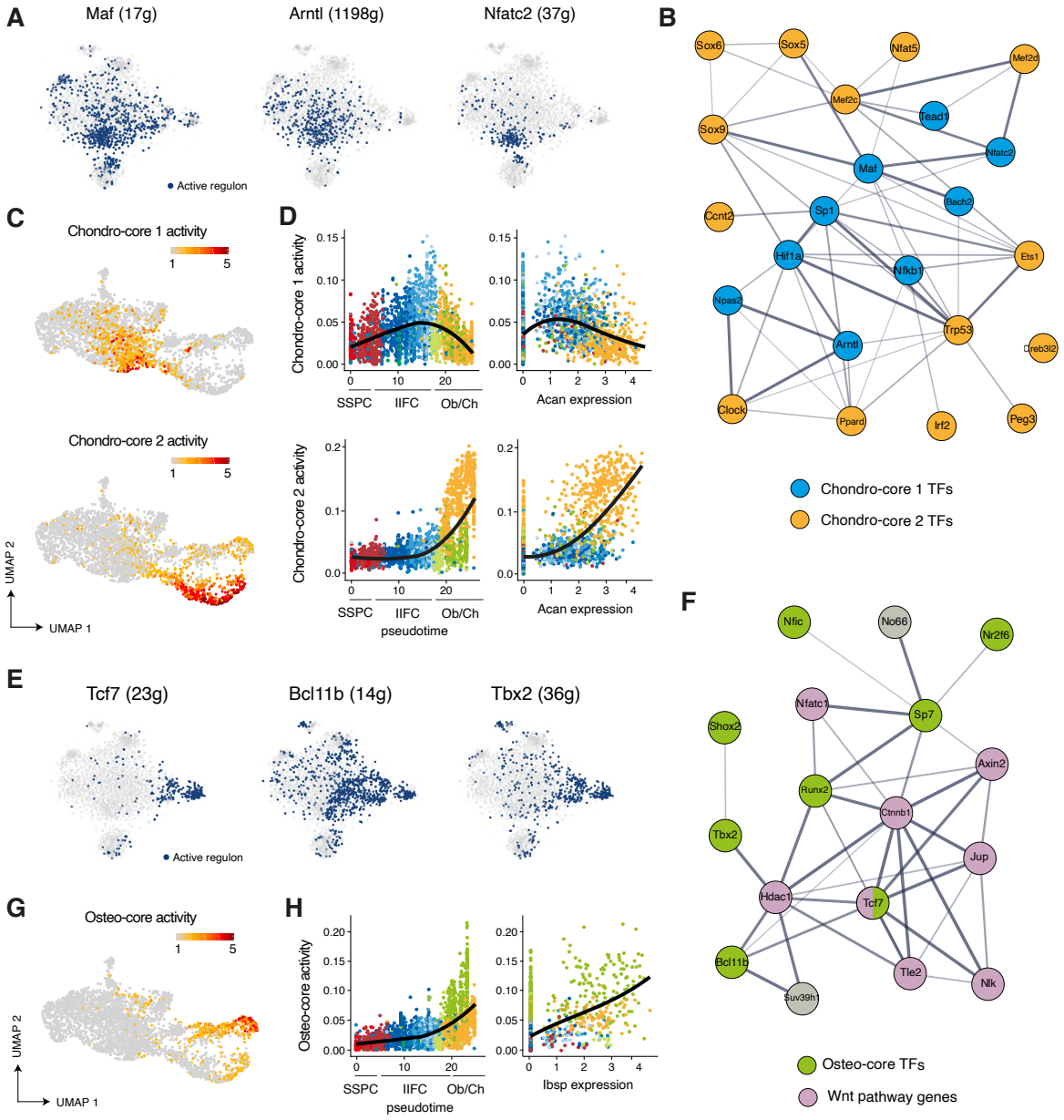

649
650

651 **Figure 7: Gene regulatory network analyses identifies gene cores driving fibrogenic to**
652 **chondrogenic and osteogenic transition.**

653 **A.** Activation of Maf, Arntl, and Nfatc2 regulons in SSPCs, IIFCs, chondrocytes and osteoblasts. **B.**
654 STRING interaction network of the chondro-core 1 and 2 transcription factors (blue and orange
655 respectively). **C.** Feature plot of chondro-core 1 (top) and chondro-core 2 (bottom) activities in SSPCs,
656 IIFCs, chondrocytes and osteoblasts in Seurat UMAP from Fig. 4. **D.** Scatter plot of chondro-core 1 (top)
657 and chondro-core 2 (bottom) activities along monocle pseudotime and *Acan* expressing. **E.** Activation
658 of Tcf7, Bclb11b and Tbx2 regulons in SSPCs, IIFCs, chondrocytes and osteoblasts. **F**. STRING
659 interaction network of the osteo-core transcription factors (green) and their related genes shows that
660 most of osteo-core related genes are involved in Wnt pathway (purple). **G.** Feature plot of the osteo-
661 core activity in SSPCs, IIFCs, chondrocytes and osteoblasts in Seurat UMAP from Fig. 4. **H.** Scatter plot
662 of osteo-core activity along monocle pseudotime and *Ibsp* expressing.
663

Figure 8

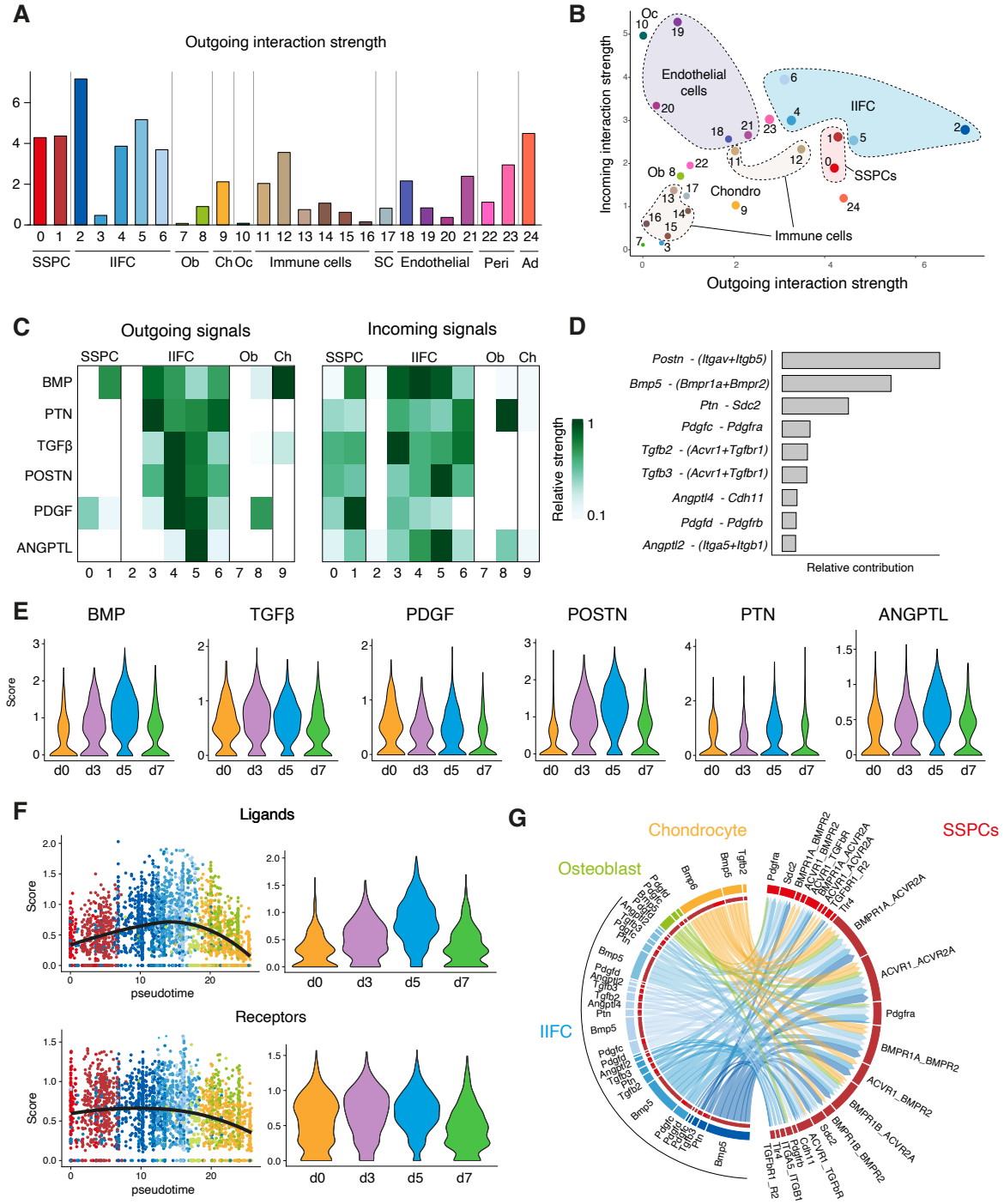
A
Outgoing interaction strength
SSPC
IIFC
Ob
Ch Oc
Immune cells
SC
Endothelial
Peri
Ad
B
Incoming interaction strength
Outgoing interaction strength
Endothelial cells
IIFC
SSPCs
Chondro
Immune cells
Oc
Ob
C
Outgoing signals
Incoming signals
SSPC
IIFC
Ob
Ch
BMP
PTN
TGFβ
POSTN
PDGF
ANGPTL
Relative strength
D
Postn - (Itgav+Itgb5)
Bmp5 - (Bmpr1a+Bmpr2)
Ptn - Sdc2
Pdgfc - Pdgfra
Tgfb2 - (Acvr1+Tgfbr1)
Tgfb3 - (Acvr1+Tgfbr1)
Angptl4 - Cdh11
Pdgfd - Pdgfrb
Angptl2 - (Itga5+Itgb1)
Relative contribution
E
BMP
TGFβ
PDGF
POSTN
PTN
ANGPTL
Score
d0
d3
d5
d7
F
Ligands
Receptors
Score
pseudotime
G
Chondrocyte
SSPCs
Osteoblast
IIFC

664

665 **Figure 8: IIFCs are the main source of paracrine factors after fracture.**

666 **A.** Outgoing interaction strengths of the different cell populations of the fracture environment determined
667 using CellChat package. **B.** Comparison of incoming and outgoing interaction strengths across SSPC,
668 IIFC, chondrogenic and osteogenic populations. **C.** Outgoing and incoming signaling from and to
669 SSPCs, IIFCs, chondrocytes and osteoblasts. **D.** Cell-cell interactions identified between SSPCs, IIFCs,
670 chondrocytes and osteoblasts. **E.** Feature plots of the score of BMP, TGFβ, PDGF, POSTN, PTN and
671 ANGPTL signaling per timepoint. **F.** Scatter plot along pseudotime and feature plot per time point of the
672 mean expression of the ligand and receptors involved in signaling from IIFCs. **G.** Circle plot of the
673 interactions between SSPCs, IIFCs, chondrocytes and osteoblasts, showing that most signals received
674 by SSPCs are coming for IIFCs.
675